Journal of Power Sources 193 (2009) 65–71

Contents lists available at ScienceDirect

Journal of Power Sources

journal homepage: www.elsevier.com/locate/jpowsour

Internal reforming characteristics of cermet supported solid oxide fuel cell using yttria stabilized zirconia fed with partially reformed methane

Akihiko Momma[a,*], Kiyonami Takano[a], Yohei Tanaka[a], Akira Negishi[a], Ken Kato[a], Ken Nozaki[a], Tohru Kato[a], Takenori Ichigi[b], Kazuyuki Matsuda[b], Takashi Ryu[b]

[a] Energy Technology Research Institute, National Institute of Advanced Industrial Science and Technology, 1-1-1 Umezono Tsukuba Ibaraki, 305-8568, Japan
[b] Application Development Project, Corporate R&D, NGK Insulators, Ltd., 2-56 Suda-cho Mizuho-ku Nagoya-shi Aichi, 467-8530, Japan

ARTICLE INFO

Article history:
Received 30 September 2008
Received in revised form
22 December 2008
Accepted 22 December 2008
Available online 31 December 2008

Keywords:
Solid oxide fuel cell
Internal reforming
Methane
Concentration measurement
Gas chromatograph

ABSTRACT

In order to investigate the internal reforming characteristics in a cermet supported solid oxide fuel cell (SOFC) using YSZ as the electrolyte, the concentration profiles of the gaseous species along the gas flow direction in the anode were measured. Partially reformed methane using a pre-reformer kept at a constant temperature is supplied to the center of the cell which is operated with a seal-less structure at the gas outlet. The anode gas is sucked in via silica capillaries to the initially evacuated gas tanks. The process is simultaneously carried out using five sampling ports. The sampled gas is analyzed by a gas chromatograph. Most of the measurements are made at the cell temperature (T_{cell}) of 750 °C and at various temperatures of the pre-reformer (T_{ref}) with various fuel utilizations (U_f) of the cell. The composition of the fuel at the inlet of the anode was confirmed to be almost the same as that theoretically calculated assuming equilibrium at the temperature of the pre-reformer. The effect of internal reforming in the anode is clearly observed as a steady decrease in the methane concentration along the flow axis. The effect of the water-gas shift reaction is also observed as a decrease in the CO_2 concentration and an increase of CO concentration around the gas inlet region, as the water-gas shift reaction inversely proceeds when T_{cell} is higher than T_{ref}. The diffusion of nitrogen from the seal-less outermost edge is observed, and the diffusion is confirmed to be more significant as U_f decreases. The observations are compared with the results obtained by the SOFC supported by lanthanum gallate electrolyte. With respect to the internal reforming performance, the cell investigated here is found to be more effective when compared to the previously reported electrolyte supported cell.

1. Introduction

Solid oxide fuel cell (SOFC) has been attracting much attention due to its high efficiency. Moreover, the variety of fuel due to its internal reforming ability has made the SOFC one of the most promising power generation systems. Well-managed utilization of its characteristics is very important for introduction of the SOFC into future markets. Especially, the effective utilization of heat is requisite in making the SOFC system compact. Many investigations have been carried out [1,2] for this purpose. In order to understand the precise characteristics of the internal reforming of SOFCs, however, experimental investigations are essential; the most effective way is to investigate the compositional change in the fuel in the anode by directly sampling the gas from the various points in the anode channel and then analyzing them.

From this point of view, first of all, Momma et al. [3] measured the gaseous composition of five different points along the fuel flow inside the anode using a practical size seal-less structure single cell (120 mm diameter) using H_2 as the fuel and lanthanum gallate as the electrolyte. As a result, by comparing the experimental data with the simulation, the validity of the experimental procedure and the simulation were mutually confirmed.

In a subsequent study [4], Momma et al. obtained information about the internal reforming of methane, water-gas shift reaction, the possible direct electrochemical reaction of CO, etc., using the same single cell as the one previously used. In the experiment, partially reformed methane was supplied through a pre-reformer kept at constant temperature and the sampled gas was analyzed by gas chromatography. These are some of the interesting findings of the experiments:

1. The reforming reaction of methane and even the water-gas shift reaction do not smoothly proceed without the existence of a properly prepared catalyst for the reaction, even in the presence of Ni.

* Corresponding author. Tel.: +81 29 861 5735; fax: +81 29 861 5805.
E-mail address: mo.momma@aist.go.jp (A. Momma).

0378-7753/$ – see front matter © 2008 Elsevier B.V. All rights reserved.
doi:10.1016/j.jpowsour.2008.12.110

Table 1
Comparison of the experimental conditions of the present cell and the previous cell.

	Previous cell type-C [4]	This work
Cell type	Electrolyte supported	Anode supported
Electrolyte	Lanthanum gallate	YSZ
Anode	Ni/SDC	Ni/YSZ
Thickness of anode (mm)	ca. 0.05	1
Anode porosity	N/A	0.4
Anode current collector	Ni foam + Ni/SDC	Ni foam
Thickness of anode current collector (mm)	1.0	0.62
Mean density of the catalyst ($kg\,m^{-3}$)	1600	2740

2. CO electrochemically reacts only when the fuel utilization becomes high and when the concentration of H_2 becomes low.
3. Because H_2 has a higher diffusivity, the H/C ratio in the anode gas rapidly decreases in the outermost region of the anode.

The next study dealt with the comparison of the simulation and the experimental data obtained from the reference [4], in which the validity of the simulation and the consideration about the above findings were discussed [5].

In the present study, a YSZ/Ni cermet supported cell with YSZ electrolyte was used instead of the lanthanum gallate cell supported by electrolyte. Analytical measurements were made by sampling the anode gas, and the results are compared with the simulation and those obtained using the previously reported lanthanum gallate cell.

2. Experimental

The SOFC used in this study is supported by 1 mm thick Ni/YSZ cermet. Its effective diameter is 120 mm and the effective area is 113 cm^2. YSZ was used as the electrolyte. The anode current collector was made of foamed Ni, the same one used in a previous study [4] in which it was denoted as type-A. The precise specifications of the present cell are listed along with those used in a previous work [4] in Table 1.

Partially reformed methane, as well as pure H_2, was used as the fuel. Methane was supplied at the flow rate of 85 $cc\,min^{-1}$ with steam (S/C = 3) to a pre-reformer kept at a constant temperature. This flow rate corresponds to 3 $cc\,min^{-1}\,cm^{-2}$ of H_2 assuming the perfect conversion of methane into H_2. The schematic of the experimental set up of the cell is illustrated in Fig. 1. The fuel and air were supplied from the center of each separator and they radially spread toward the outer most edge of each electrode where the gases spread into the outside air. At the same time, the sealless structure allowed the diffusion of the outside air into the gas channels. The gas channel of the anode in this study consisted of a porous Ni/YSZ cermet and porous anode current collector. T_{cell} was measured and controlled by thermocouples inserted into the center area of each separator.

The measurements were carried out for various U_f values as defined by Eq. (1).

$$U_f = \frac{\text{output current}}{\text{current needed to completely spend 340 cc min}^{-1}\text{ of H}_2\text{ by the fuel cell reaction}} \times 100 \quad (1)$$

in which 340 $cc\,min^{-1}$ of H_2 corresponds to the complete conversion of methane supplied at the rate of 85 $cc\,min^{-1}$. The experimental conditions are summarized in Table 2.

2.1. Generation of partially reformed methane

The mixture of steam and methane was supplied to the pre-reformer which was separately equipped outside the housing of the cell. Al_2O_3 supported Ru was used as the catalyst for the reforming reaction. The temperature at the downstream of the catalyst embedded region of the reformer was controlled and recorded. Steam was generated by introducing the pre-degassed water into the boiler of which temperature and pressure were controlled. The flow rate of the degassed water was controlled by a solution-sending pump (TOSOH CCPS) which can control the flow rate down to 1 $\mu L\,min^{-1}$. The flow rate of the water was monitored and checked by weighing the water reservoir from which water was removed.

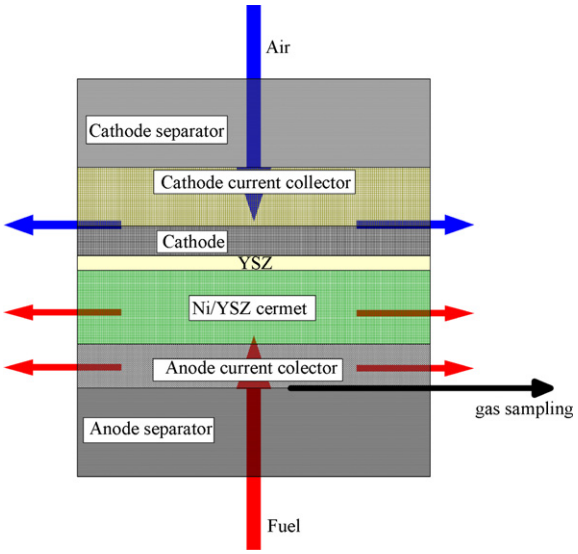

Fig. 1. Schematic of the cell assembly configuration for the measurements.

2.2. Sampling of the gas

Sampling of the gas from the anode gas channel was carried out via capillary tubes made of silica (150–200 μm I.D.). The capillary tubes were embedded in the ditches made on the surface of the anode separator. The tips of the capillaries from which the gas was sucked and sampled were placed at the radial positions of r = 0 mm, 14 mm, 28 mm, 42 mm and 56 mm. The position of the tips was circumferentially shifted in order to minimize the effect of the sampling of the upstream region on the sampling of the downstream region. The sampling from the five points was simultaneously conducted using the initially evacuated tanks kept at 150 °C at the rate of ca. 2 $cc\,min^{-1}$/each until the pressure of the tanks became ca. 0.2 atm.

2.3. Analysis procedure

A schematic of the experimental set was previously illustrated [4]. The sampled gases were diluted by Ar to about 1/20 and pressurized. This dilution made it possible to introduce the sampled gas into the analyzers by utilizing the pressure without the water condensation. It also made the concentration of steam in the sampled gas dilute enough to analyze using a gas chromatograph. The pressurized sampled gases were then sequentially introduced analyzers. A micro-gas chromatograph (mGC, Agilent Technologies, Agilent 3000 micro GC) was used for the analysis. A quadrupole mass spectrometer (QMS, Anelva M-200GA-DM) was used for the auxiliary purposes for real time qualitative monitoring during the measurements. Necessary

Table 2
Experimental conditions and experimentally obtained concentration of gaseous species at the inlet of the anode.

T_{cell} (°C)	Fuel	Flow rate (cc min^{-1})	S/C	T_{ref} (°C)	U_f (%)	H_2 (r=0) (%)	H_2O (r=0) (%)	CH_4 (r=0) (%)	CO (r=0) (%)	CO_2 (r=0) (%)
750	H_2	340	–	–	0	100	0	0	0	0
750	CH_4	85	3.0	600	0	51.2	30.2	4.3	5.3	8.8
750	CH_4	85	3.0	600	50	51.2	30.4	4.2	5.3	8.8
750	CH_4	85	3.0	600	70	51.2	30.4	4.2	5.3	8.8
750	CH_4	85	3.0	550	0	43.8	36.7	7.7	2.8	8.8
750	CH_4	85	3.0	550	50	43.8	36.7	7.6	2.8	8.9
750	CH_4	85	3.0	550	70	42.7	38.0	7.5	2.8	8.8
750	CH_4	85	3.0	500	0	35.0	44.0	11.4	1.2	7.9
750	CH_4	85	3.0	500	70	35.0	43.9	11.5	1.2	7.9
800	CH_4	85	3.0	500	70	34.9	44.2	11.4	1.3	7.8
Calculated gas composition at T_{ref} = 600 °C						50.1	31.8	4.3	5.1	8.7
Calculated gas composition at T_{ref} = 550 °C						42.9	37.8	7.9	2.7	8.7
Calculated gas composition at T_{ref} = 500 °C						34.2	45.2	11.7	1.1	7.7

heating (>150 °C) and heat insulating of the tubing were utilized.

Table 3 shows the configuration of the mGC used for the analysis. It has four channels that work in parallel and it allows the analysis of the most likely species in this experiment. All the columns were supplied by Agilent Technologies.

2.4. Calibration of mGC

Calibration of the mGC was carried out prior to the measurements. The calibration method and some of the results are shown elsewhere [4]. Because it is not typical to use gas chromatography for the analysis of steam, careful attention was made for the confirmation of linearity of the mGC versus the steam concentration. By supplying various concentrations of $H_2O + H_2$ mixtures diluted by Ar, the linearity was investigated. The results obtained by the mGC showed a good correlation with the QMS results and showed good linearity, indicating the validity of the quantitative analysis of steam by the mGC. Thus the concentration of each gaseous species was decided to be obtained by one point calibration of the mGC using standard gas and the prescribed $H_2 + H_2O$ mixture diluted by Ar.

3. Modeling of the simulation

The detailed modeling of the simulation has been described in the literature [5,6] in which utilizations of the catalyst were expressed as α_{ref} and α_{sf} for the reforming (4) and water-gas shift (5) reactions, respectively.

$$\rho_{cat,ref} = \rho_{anc} \times \alpha_{ref} \quad (2)$$

$$\rho_{cat,sf} = \rho_{anc} \times \alpha_{sf} \quad (3)$$

$$CH_4 + H_2O \rightarrow CO + 3H_2 \quad (4)$$

$$CO + H_2O \rightarrow CO_2 + H_2 \quad (5)$$

where ρ_{anc} is the density of the anode current collector in kg m^{-3}, $\rho_{ca,ref}$ and $\rho_{cat,sf}$ are the densities of the catalysts which actually contribute to the reforming and water-gas shift reactions in kg m^{-3}, respectively.

These values had been determined by comparing the experimental data with the simulation curves calculated by assuming various α_{ref} and α_{sf} values. Using the same procedure, in this study, the values were found to be identical to those previously reported for the current collector type-C: $\alpha_{ref} = \alpha_{sf} = 0.03$. The value corresponds to 82 kg m^{-3} and 130 g m^{-2} for the catalyst which effectively exists in the anode gas channel.

Table 3
Configuration of micro-gas chromatograph used for the measurement.

Channel	Column type	Carrier gas	Back-flush injection	Detectable species
#1	Molsieve	Ar	Yes	H_2, N_2, CH_4, CO
#2	Molsieve	He	Yes	Ar, N_2, CH_4, CO
#3	PoraPlotQ	He	Yes	Ar, CO_2
#4	OV-1	He	No	Ar, H_2O

4. Results and discussion

4.1. Comparison of concentration profile using pure H_2 as a fuel

The results of the measurements at U_f = 0% using H_2, instead of methane, as a fuel are shown in Fig. 2 along with the results obtained using the previously reported lanthanum gallate cell [3]. H_2 supplied from the center of the cell decreased more rapidly in the case of the lanthanum gallate cell than in the present case and the increase in the steam concentration became steeper, accordingly. This was explained by the presence of the electronic conduction in the lanthanum gallate assuming the electronic transference number to be 0.7% in our previous study [3]. There are several reports concerning the electronic conductivity of the lanthanum gallate. Ishihara et al. [7] reported much smaller transference number for the electronic conduction. The difference shown in Fig. 2 cannot be explained by the electronic conduction in the electrolyte if the value reported by Ishihara et al. applies for the present case. On the other hand, much larger value was reported by Kuroda et al. [8] in

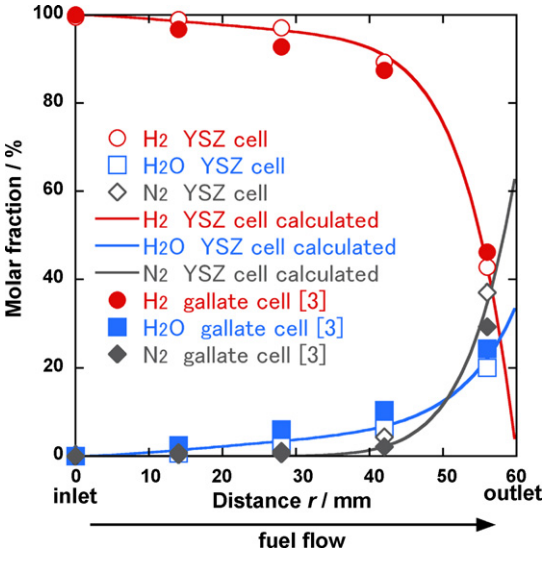

Fig. 2. Comparison of the concentration profiles obtained by pure H_2 as a fuel with the present cell (open symbols) and with the previously reported cell (solid symbols) at U_f = 0% and T_{cell} = 750 °C. Solid lines denote the simulated curves for the present YSZ cell.

which they suggested that the preparation of the electrolyte might influence the measured electronic transference number. It cannot be denied that the heat treatments and possible reaction with electrode materials during the cell formation might have slightly changed the electronic behavior in the lanthanum gallate of the present study.

In Fig. 2, it can be seen that in the case of the anode support cell, because the gas channel is thicker, the diffusion of N_2 from ambient at the outermost edge became more significant. However, in either case, the diffusion at the outlet region made the local electromotive force (emf) extremely low. This produced the large distribution of the local emf inside the cell, which caused the electrolysis current at around the outermost edge of the cell. This, in turn, generated the fuel cell current in the inner region, compensating for the electrolysis current because the total output current must be zero. This made the simple qualitative explanation of the concentration profile in the anode quite difficult.

In the figure, the simulated curves based on the present cell (YSZ cell) are also shown by the solid lines. The very good agreement between the experimental data and the simulation indicates the validity of the assumptions for the simulation under the present experimental conditions.

4.2. Composition at the anode inlet

In Table 2, the measured gaseous compositions at the inlet of the cell, i.e., $r = 0$ mm, are shown along with the calculated composition assuming equilibrium at the pre-reformer temperature. The observed compositions are quite close to the calculated ones, which means that the partially reformed methane of the equilibrium composition at the reformer temperature was supplied to the inlet of the anode with only a very slight compositional change in the tubing between the pre-reformer and the cell. This is because the time required for the pre-reformed gas to pass through the tubing was quite short due to the small volume of the tubing. The absence of the appropriate catalyst in the tubing could be another reason for this, because it was found that even in the presence of Ni, the reforming reaction did not proceed without the presence of the appropriate catalyst [4].

4.3. Partially reformed methane: comparison of different cells

When partially reformed methane is used for the fuel, it is quite natural to expect that the internal reforming reaction is fast using the present cell because it has a thick anode which may work as a catalyst.

To clarify the difference of the catalytic activities among the various cells, the obtained concentration profile of methane is shown with the previously obtained results [4] at $T_{ref} = 550\,^{\circ}C$ and $U_f = 0\%$ in Fig. 3. With the present cell, the concentration of the non-reformed methane decreased to ca. 1/2 of that at the inlet when the gas reaches $r = 14$ mm. It should be noted that the velocity of the gas is extremely fast at around the inlet region and it only takes a very short time to reach $r = 14$ mm. This indicates the obvious superiority of the present cell in terms of the catalytic activity for the reforming reaction over the previously reported cell. The obtained values of $130\,g\,m^{-2}$ stated above means that about a 3 times higher amount of effective catalyst existed per unit area of the anode compared to that in the previous cell using the type-C current collector. This difference in the amount of the effective catalyst can be concluded to make a difference in the internal catalytic performance shown in Fig. 3.

In Fig. 4 the concentration profiles of H_2 obtained with the different types of cells are shown at $T_{ref} = 550\,^{\circ}C$ and $U_f = 0\%$. Due to the absence of an external current, the comparison of the difference in the increase of the H_2 concentration due to the reforming

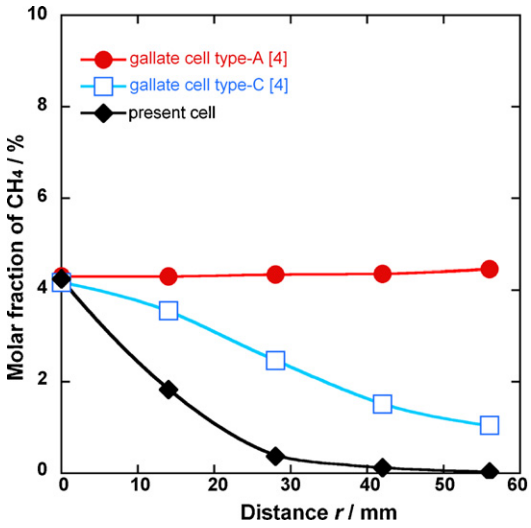

Fig. 3. Comparison of the concentration profiles of methane obtained at $T_{ref} = 550\,^{\circ}C$, $T_{cell} = 750\,^{\circ}C$ and $U_f = 0\%$ for various type of cells.

of methane is relatively easy. Nevertheless, it should be noted that there existed an internal fuel cell current that flowed to compensate the electrolysis current which may appear in the region where the local emf became lower than the cell voltage. There was also H_2 consumption due to the electronic conduction in the electrolyte when using the lanthanum gallate cells.

The results of the CO concentration profile obtained at $T_{ref} = 550\,^{\circ}C$ and $U_f = 0\%$ are also shown in Fig. 5. Because the temperature of the pre-reformer was 550 °C and that of the cell was 750 °C, the partially reformed methane which equilibrated at the pre-reformer temperature of 550 °C, when it was introduced to the cell, was expected to proceed in the reverse of Eq. (5). Therefore, the CO concentration was expected to increase. Although in the case of the lanthanum gallate cell using the current collector type-A, the increase in the CO concentration was scarcely observed, in the case of the present cell, the concentration of CO was found to rapidly increase as it was supplied from the center and spread through the channel. The concentration of CO and CO_2 became almost equal to their equilibrium values when the fuel reaches $r = 28$ mm. The time required for the fuel to reach $r = 28$ mm can be calculated to be approximately 70 ms.

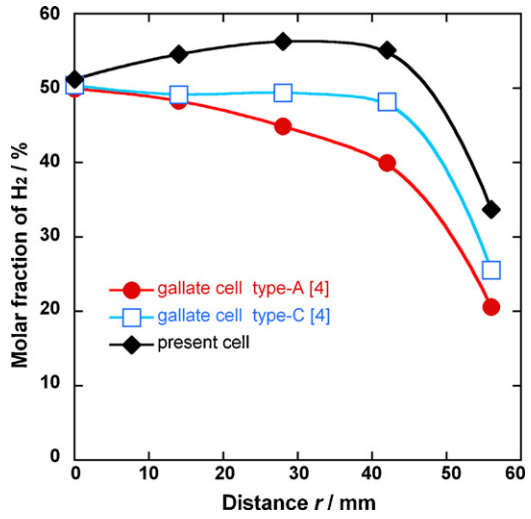

Fig. 4. Comparison of the concentration profiles of H_2 obtained at $T_{ref} = 550\,^{\circ}C$, $T_{cell} = 750\,^{\circ}C$ and $U_f = 0\%$ for various type of cells.

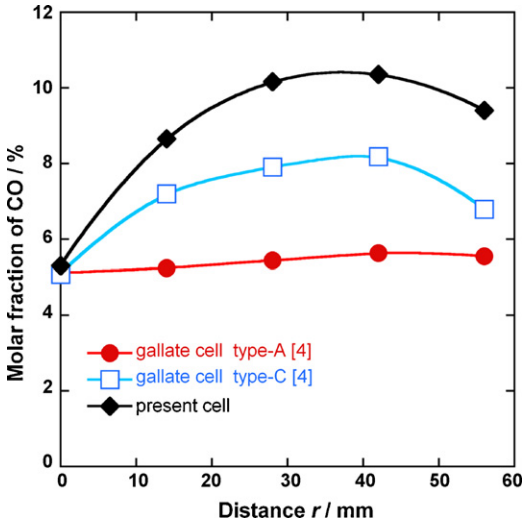

Fig. 5. Comparison of the concentration profiles of CO obtained at T_{ref} = 550 °C, T_{cell} = 750 °C and U_f = 0% for various type of cells.

4.4. Concentration profile at various T_{ref} and U_f values

In Fig. 6, the comparisons of the experimental data and the simulation are shown for various T_{ref} values under U_f = 70%. The experimental value at r = 28 mm could not be obtained at T_{ref} = 500 °C due to technical problems. Because the parameters α_{ref} and α_{sf} for the simulation were fitted using the data obtained at T_{ref} = 500 °C, the best fit was realized at this condition. Nevertheless, considerably good agreements can also be seen both at T_{ref} = 550 °C and T_{ref} = 600 °C. In the figures, the calculated local cell emf and local current density J_0 are also shown as well as the gaseous species concentration profiles. Due to the diffusion of the ambient air into the anode at the periphery of the disc, the sudden decrease in the emf can be seen in the outermost region where the concentration of fuel also rapidly decreases.

Even though the direct electrochemical reaction of CO was not considered in the present simulation, the excellent agreement in the concentration of CO and CO_2 between the experimental and the calculated values, especially in the outlet region, supports the previously reported findings [4], i.e., the direct reaction of CO becomes noticeable only when the internal reforming characteristics of the anode are poor and when H_2 is depleted by the cell reaction in the outlet region.

In Fig. 7, the comparisons of the experimental data and the simulation are shown for U_f = 0% (Fig. 7(a)) and U_f = 50% (Fig. 7(b)). It can be seen that the simulation agrees quite well with the experiment regardless of U_f. The comparison of the figures including Fig. 6(c) revealed that the diffusion of N_2 into the anode became more significant as U_f decreased. This is because the concentration of H_2 becomes greater in the outlet region as U_f decreases and because the mutual diffusion of H_2–N_2 takes place quite easily.

The previous simulations [3,5] have shown that the large drop in the local emf at the outlet region caused the reversal of the cell voltage and the local emf and, hence, to the occurrence of the electrolysis current at the outlet region. On the other hand, the present simulation predicted the generation of the electrolysis current not only at the outlet region, but also at the inlet region.

In Fig. 8, the calculated distribution of the local current density was plotted at various pre-reformer temperatures for U_f = 0%. The figure indicates that when T_{ref} is low along with a low conversion of methane, the reversal of the local emf and the cell voltage occurs at the inlet region due to the low H_2 concentration and high H_2O concentration. This reversal causes the electrolysis current at the

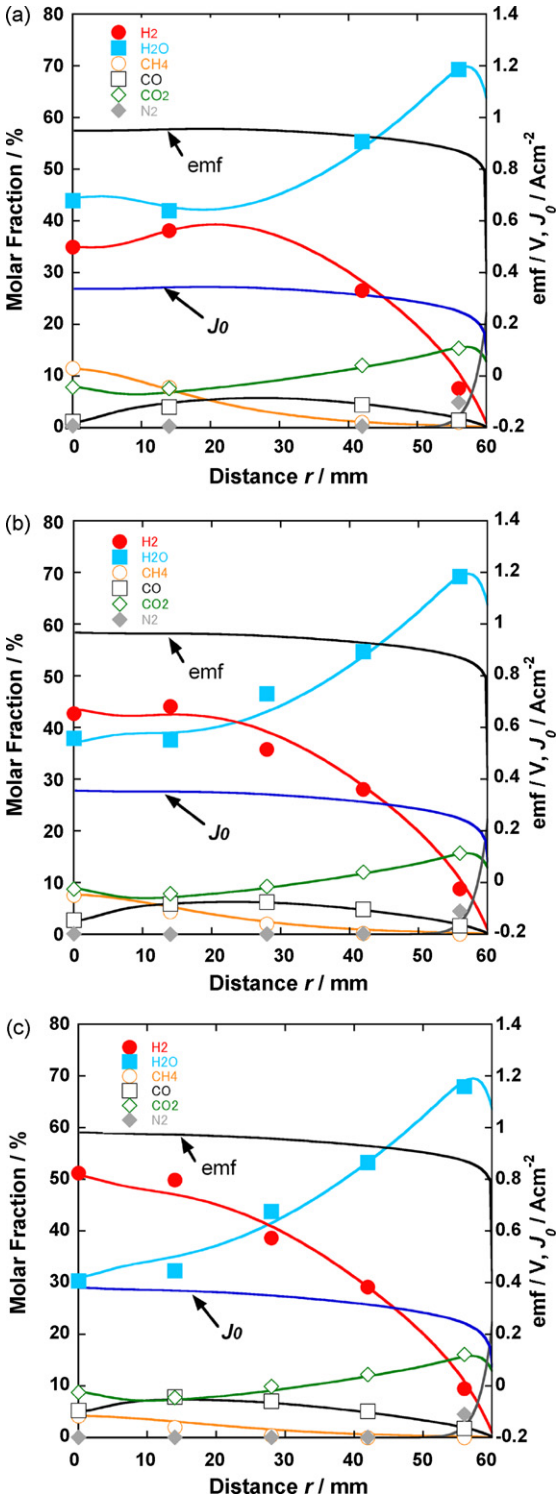

Fig. 6. Comparison of the experimental data and the simulation at various T_{ref} values at T_{cell} = 750 °C and U_f = 70%. (a) T_{ref} = 500 °C, (b) T_{ref} = 550 °C, (c) T_{ref} = 600 °C.

inlet region. This electrolysis current at the inlet region was not predicted for the previously reported cases. There are two reasons for this: one of the reasons is that the previous report dealt with the cell made of electrolyte that has electronic conduction and hence the cell voltage was suppressed. The second reason is that the catalytic activity of the previously reported cell was not good enough, which also made the cell voltage low. The low cell voltage caused the reversal of cell voltage and local emf less likely to appear.

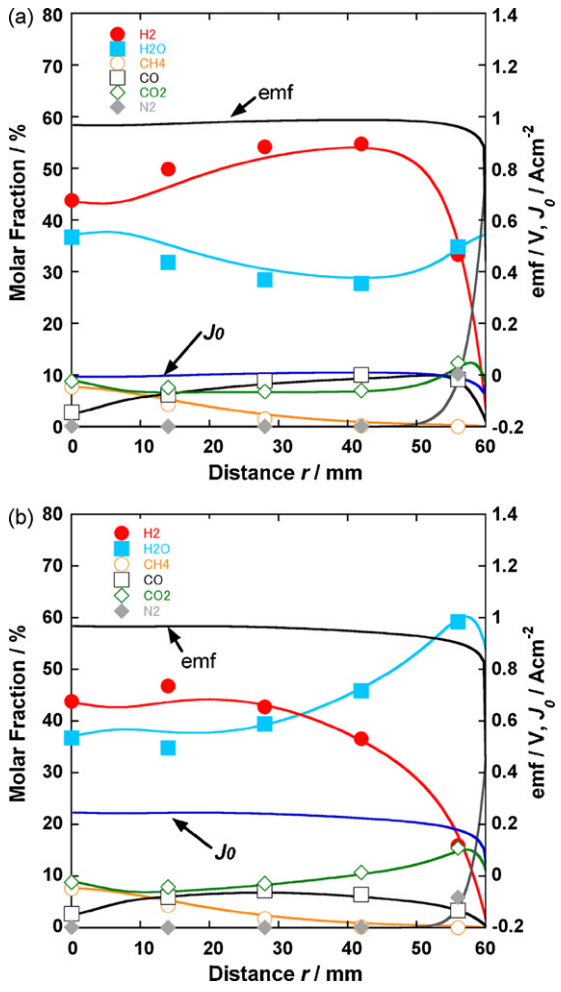

Fig. 7. Comparison of the experimental data and the simulation at T_{ref} = 550 °C and T_{cell} = 750 °C under (a) U_f = 0% and (b) U_f = 50%.

Both of the reasons mentioned above refer to the relative difference between the cell voltage and the local emf; if the cell voltage is high, the reversal of the local emf and cell voltage is likely to take place, leading to the occurrence of the electrolysis current. Therefore, it should be strongly noted that the significant electrolysis current at the inlet of the cell could occur, especially with the cell that has a sealed structure at the gas outlet.

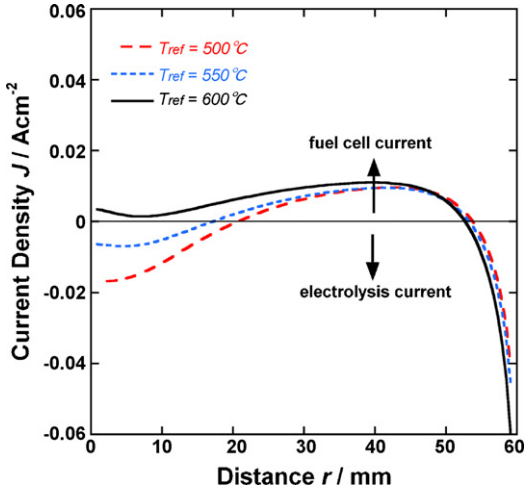

Fig. 8. Distribution of the calculated local current density at T_{cell} = 750 °C with U_f = 0% at various T_{ref} values.

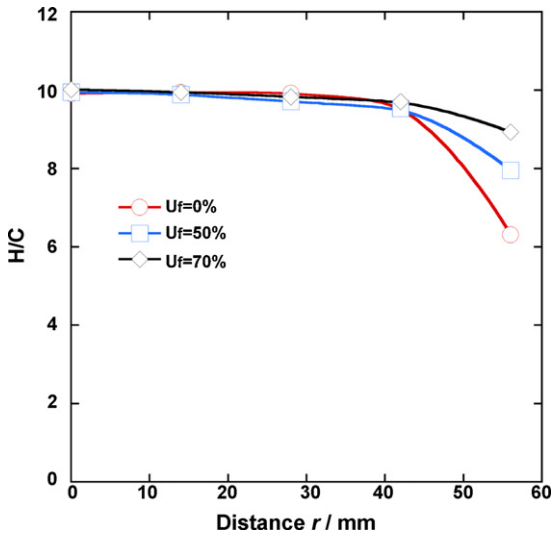

Fig. 9. Distribution of H/C ratio experimentally obtained for various U_f values at T_{ref} = 550 °C and T_{cell} = 750 °C.

In Fig. 9, the profile of the experimentally obtained H/C ratio, defined as $H_{balance}/C_{balance}$ in Ref. [4], is shown. The H/C ratio equals 10 at the inlet which reflects the input gaseous ratio of S/C = 3. The H/C ratio at the outlet region suddenly decreased and the degree of this decrease became greater as U_f decreased. This phenomenon is attributable to the difference in the diffusivity among the gaseous species; H_2, which diffused faster than any other species, easily flowed out of the cell while the other species containing C stayed longer and slowly decreased.

5. Conclusion

The investigations of the internal reforming characteristics of SOFC supported by the Ni/YSZ cermet were carried out by analyzing the compositions of the gaseous species along the gas flow in the anode, and the following conclusions were obtained.

1. Internal reforming proceeded very smoothly. Even when the temperature of the pre-reformer was 500 °C with a relatively high concentration of non-reformed methane at the inlet, methane was found to be reformed almost completely by the outlet of the cell. The comparison of the simulation has clarified that the amount of the effective catalyst was about 3 times higher than those previously reported for the lanthanum gallate cell.
2. The progress of the water-gas shift reaction was also found to be quite smooth and the equilibrium was almost attained until the gas reaches r = 28 mm which corresponds to ca. 70 ms.
3. It was predicted that when U_f is very low, the reversal of the local emf and cell voltage, not only around the outermost edge of the cell, but also at around the inlet region of the cell, occurred. The phenomenon became noticeable when the electrolyte has no electronic conduction, when the catalytic activity of the cell is good and when the S/C ratio is high. This led to the occurrence of an electrolysis current at the inlet region as well as at the outlet region.
4. At the outlet region, because of the difference in the diffusivity of the gaseous species, H_2 diffused faster than any other species and the H/C ratio in the anode decreased accordingly.

In addition to these conclusions, the procedures applied here have been found to provide an intensive method for evaluating the internal reforming of SOFCs.

Acknowledgement

This study was supported by the Ministry of Economy Trade and Industry of Japan. The authors are grateful for the financial support.

References

[1] R. Peters, R. Dahl, U. Kluttgen, C. Palm, D. Stolten, J. Power Sources 106 (2002) 238–244.
[2] V.M. Janardhanan, V. Heuveline, O. Deutschmann, J. Power Sources 172 (2007) 296–307.
[3] A. Momma, Y. Kaga, K. Takano, K. Nozaki, A. Negishi, K. Kato, T. Kato, T. Inagaki, H. Yoshida, K. Hoshino, M. Yamada, T. Akbay, J. Akikusa, J. Power Sources 145 (2005) 169–177.
[4] A. Momma, K. Takano, Y. Tanaka, A. Negishi, K. Kato, M. Amano, K. Nozaki, T. Kato, T. Inagaki, M. Kawano, K. Hosoi, K. Hoshino, M. Shibata, T. Akbay, J. Akikusa, N. Chitose, ECS Trans. 7 (2007) 805–814.
[5] T. Shimada, A. Momma, K. Takano, T. Kato, J. Power Sources 187 (2009) 8–18.
[6] K. Takano, S. Nagata, K. Nozaki, A. Momma, T. Kato, Y. Kaga, A. Negishi, K. Kato, T. Inagaki, H. Yoshida, K. Hosoi, K. Hoshino, T. Akbay, J. Akikusa, J. Power Sources 132 (2004) 42–51.
[7] T. Ishihara, S. Ishikawa, C. Yu, T. Akbay, K. Hosoi, H. Nishiguchi, Y. Takita, Phys. Chem. Chem. Phys. 5 (2003) 2257–2263.
[8] K. Kuroda, I. Hashimoto, K. Adachi, J. Akikusa, Y. Tamou, N. Komada, T. Ishihara, Y. Takita, Solid State Ionics 132 (2000) 199–208.